Crystal structure and physical properties of radical cation salt based on 4,5-ethylenedioxy-4′-iodotetrathiafulvalene (EDO-TTF-I) with iodine bonding ability

AUTHOR(S):

Nakano, Yoshiaki; Takahashi, Yusuke; Ishida, Kohdai; Ishikawa, Manabu; Yamochi, Hideki; Uruichi, Mikio

CITATION:

Nakano, Yoshiaki ...[et al]. Crystal structure and physical properties of radical cation salt based on 4,5-ethylenedioxy-4′-iodotetrathiafulvalene (EDO-TTF-I) with iodine bonding ability. Materials Chemistry Frontiers 2018, 2(4): 752-759

ISSUE DATE:

2018-01-29

URL:

http://hdl.handle.net/2433/230372

Crystal structure and physical properties of radical cation salt based on 4,5-ethylenedioxy-4'-iodotetrathiafulvalene (EDO-TTF-I) with iodine bonding ability

Yoshiaki Nakano,[*ab] Yusuke Takahashi,[a] Kohdai Ishida,[a] Manabu Ishikawa,[b] Hideki Yamochi[ab] and Mikio Uruichi[c]

[a.] Department of Chemistry, Graduate School of Science, Kyoto University, Kitashirakawa Oiwake-cho, Sakyo-ku, Kyoto 606-8502, Japan.

[b.] Research Center for Low Temperature and Materials Sciences, Kyoto University, Yoshida Honmachi, Sakyo-ku, Kyoto 606-8501, Japan.

[c.] Institute for Molecular Science, Myodaiji, Okazaki, Aichi 444-8585, Japan.

E-mail: nakano.yoshiaki.5x@kyoto-u.ac.jp (Y. Nakano).

Electronic Supplementary Information (ESI) available: Crystallographic data, crystal structures, overlap integrals, energy band structures, Fermi surfaces, sample dependence on the electrical resistivity, temperature dependence of the magnetic susceptibility fitted by Bonner−Fisher model, and infrared/Raman spectra and frequencies of EDO-TTF-I. CCDC 1590291−1590294. See DOI: 10.1039/x0xx00000x

Abstract

Single crystals of 4,5-ethylenedioxy-4'-iodotetrathiafulvalene (EDO-TTF-I) with iodine bonding ability were obtained by recrystallization from acetonitrile and crystallized in the orthorhombic system with the space group *Pbca*. Bent EDO-TTF-I molecules formed the dimer structure, and a short I···O contact was observed between dimers. Electrocrystallization of EDO-TTF-I in absolute ethanol containing tetrabutylammonium hexafluorophosphate, (TBA)PF_6, afforded single crystals of (EDO-TTF-I)$_2PF_6$. An X-ray structural analysis revealed that EDO-TTF-I molecules form dimerized stacking columns in a head-to-tail manner, which is referred to as a β'-type arrangement. Iodine bonds between EDO-TTF-I and PF_6 anions and short I···S contacts between EDO-TTF-I molecules were observed. Tight-binding band calculations indicated that the strong molecular dimerization splits the energy band into upper and lower bands with a small energy gap, where the upper band is effectively half-filled. It was found that (EDO-TTF-I)$_2PF_6$ is semiconducting (σ_{RT} = 5.3 S cm^{-1} and E_a = 0.17 eV) and exhibits magnetic properties reminiscent of a low-dimensional localized spin system. The magnetic data were analyzed by the Bonner−Fisher model incorporating interchain interactions: $|J|/k_B$ = 67.1 K and zJ'/k_B = −61.1 K. No splitting of the C=C stretching modes was observed in the range of 5−300 K by Raman spectroscopy, indicating a homogeneous charge distribution of EDO-TTF-I$^{0.5+}$. Therefore, (EDO-TTF-I)$_2PF_6$ is considered as a dimerized Mott insulator.

Introduction

The concept of crystal engineering is attractive for controlling molecular arrangements. Supramolecular noncovalent interactions such as hydrogen and halogen bonds have been effectively utilized in order to develop molecular conductors since the bulk physical properties are dominated by the crystal structure.[1] A halogen bond is formed in the manner of C−Hal···B (Hal = F, Cl, Br, or I; B = Lewis base) when a Lewis base comes close to a halogen. This originates from the anisotropy of the electron density around the atomic nucleus of a halogen, around which electron-rich and -poor regions exist in the directions across and along bonding axis, respectively. As a result, the electron-poor region (a so-called σ-hole) of

a halogen electrostatically interacts with the electron-rich region of a Lewis base. Therefore, the halogen bond is highly directional, and iodine, which is the most polarizable, forms the most directional and strongest halogen bond.[2] In addition to these characteristics, the electronegativity of iodine is smaller than that of carbon, unlike the other halogens according to the Allred−Rochow scale: I (2.21) < C (2.50) < Br (2.74) < Cl (2.83) < F (4.10).[3] The low electronegativity does not cause a noticeable decrease in the electron donation properties, even if iodine is introduced into some donor molecule. On the basis of such characteristics, iodine-containing molecular conductors have been developed to construct unique structures and physical properties.[4,5,6]

Previously, we reported that 4,5-ethylenedioxytetrathiafulvalene (EDO-TTF) affords a radical cation salt that undergoes a thermal metal−insulator transition accompanied with distinct molecular deformation, which is driven cooperatively by the Peierls, charge-ordering, and anion-ordering mechanisms.[7a,d] Furthermore, an ultrafast and highly efficient photoinduced phase transition in this salt was discovered,[7b] and a detailed picture of the dynamic process in a nonequilibrium state,[7j] which is different from the thermal equilibrium state, is being clarified by time-resolved spectroscopies[7c,e,g,h] and electron diffraction.[7f,i] In order to develop another functional system based on an EDO-TTF derivative, we focused on 4,5-ethylenedioxy-4’-iodotetrathiafulvalene (EDO-TTF-I) with the iodine bonding ability mentioned above. EDO-TTF-I is a known donor molecule, as is the diiodonated derivative EDO-TTF-I_2. Although various complexes with EDO-TTF-I_2 have been investigated,[5a-d,6a-d,8] those with EDO-TTF-I have not been well-studied. Only semiconducting (EDO-TTF-I)$_2$(TCNQ) has been reported to the best of our knowledge, where TCNQ stands for 7,7,8,8-tetracyanoquinodimethane.[6a,8] Here, we report the crystal structure and physical properties of a radical cation salt based on EDO-TTF-I.

Results and discussion

Crystal and band structures

EDO-TTF-I was prepared through the iodination of EDO-TTF according to a slightly modified method in the literature.[8] EDO-TTF was lithiated with a slight excess of lithium diisopropylamide (LDA) in

tetrahydrofuran (THF), followed by reaction with perfluorohexyl iodide to afford EDO-TTF-I. Single crystals of EDO-TTF-I suitable for X-ray structural analysis were obtained by recrystallization from acetonitrile. EDO-TTF-I crystallizes in the orthorhombic system with the space group *Pbca* (Table 1). One EDO-TTF-I molecule is crystallographically unique, and bent EDO-TTF-I molecules form a dimer structure (Figs. 1a and S1). Regarding the short atomic contact of an iodine atom, short I15···O12 contacts of 3.324(2) Å [3.429(4) Å] with a C8−I15···O12 angle of 160.36(8)° [160.1(1)°] and a I15···O12−C9 angle of 115.0(1)° [112.1(3)°] were observed at 100 K [300 K] between the dimers (Fig. 1b).

The galvanostatic electrocrystallization of EDO-TTF-I in absolute ethanol containing tetrabutylammonium hexafluorophosphate, $(TBA)PF_6$, afforded black crystals of $(EDO\text{-}TTF\text{-}I)_2PF_6$. $(EDO\text{-}TTF\text{-}I)_2PF_6$ crystallizes in the triclinic system with the space group $P\bar{1}$ (Table 1). The PF_6 anion is located at the center of inversion, and one EDO-TTF-I molecule and one half of a PF_6 anion are crystallographically unique (Fig. S2). The arrangement of EDO-TTF-I molecules and the notation of the intermolecular overlap integrals between the highest occupied molecular orbitals (HOMOs) are shown in Fig. 2. EDO-TTF-I molecules form a dimerized stacking column along the *b* axis in a head-to-tail manner (Figs. 3a and S3). In the face-to-face stack, ring-over-bond (*s*1) and ring-over-atom (*s*2) overlapping modes alternate (Figs. 3a and S4); this molecular arrangement is known as *β′* type in BEDT-TTF conductors.[9] Focusing on the iodine-mediated intermolecular interaction, short I15···F19 contacts of 3.102(2) Å [3.202(5) Å] with a C8−I15···F19 angle of 172.25(9) [172.0(1)°] and a I15···F19−P16 angle of 114.56° [114.9°] were observed, and I15···S6 contacts of 3.6617(8) Å [3.712(1) Å] with a C8−I15···S6 angle of 91.52(8) [91.9(1)°], a I15···S6−C2 angle of 165.2(1) [164.1(1)°], and a I15···S6−C10 angle of 85.3(1) [85.6(2)°] were observed at 100 K [300 K] (Fig. 3b). A similar manner of short atomic contacts has been reported for $(EDT\text{-}TTF\text{-}I)_2Ag(CN)_2$ and $(EDT\text{-}TTF\text{-}I)_2Br$.[10] Therefore, the monoiodinated tetrathiafulvalene skeleton seems to induce the C−I···anion and C−I···S interactions and the dimerized stack with a ring-over-bond stacked dimer as a structural unit, although it is absolutely necessary to intensively research the crystal structures of monoiodinated tetrathiafulvalene radical cation

salts.

From the intradimer and interdimer overlap integrals $s1$ and $s2$ ($s1 > s2$), the degree of molecular dimerization along the stacking direction ($\Delta s/\langle s\rangle$) is defined as[11]

$$\Delta s/\langle s\rangle = 2(s1 - s2)/(s1 + s2) \qquad (1)$$

The degree of molecular dimerization in $(EDO\text{-}TTF\text{-}I)_2PF_6$ is summarized in Table S1. Judging from the values of $\Delta s/\langle s\rangle$ without the sulfur 3d orbitals, the molecular dimerization is comparable to those in $(TMTTF)_2PF_6$ and $(TMTTF)_2AsF_6$, which are in the dimerized Mott state.[12] In the case of $(TMTTF)_2PF_6$ and $(TMTTF)_2AsF_6$, the degree of molecular dimerization decreases as the temperature decreases, whereas that in $(EDO\text{-}TTF\text{-}I)_2PF_6$ increases. The energy band structure and Fermi surface are shown in Figs. 4 and S5. The strong molecular dimerization splits the energy band into upper and lower bands, although the energy gap (E_g) is very small (Table S1). Considering only the upper band, an effective half-filled band is realized. The Fermi surface calculated without the sulfur 3d orbitals is slightly open along the k_a direction, indicating a quasi-one-dimensional nature. However, the direction of opening in the Fermi surface is quite different from that calculated with the sulfur 3d orbitals (Fig. S5). The anisotropic nature will be examined in the future.

Electrical and magnetic properties

The electrical resistivity of $(EDO\text{-}TTF\text{-}I)_2PF_6$ was measured along the b axis corresponding to the stacking direction. The temperature dependence of the electrical resistivity is shown in Fig. S6. $(EDO\text{-}TTF\text{-}I)_2PF_6$ exhibits semiconducting behavior with an electrical conductivity of 5.3 S cm^{-1} at room temperature with an activation energy E_a = 0.17 eV.

The temperature dependence of the magnetic susceptibility (χ) of $(EDO\text{-}TTF\text{-}I)_2PF_6$ is shown in Figs. 5 and S7. The value of χ is 7.1×10^{-4} emu mol^{-1} at 300 K, increases as the temperature decreases, and decreases through the maximum at 85 K. The magnetic behavior is reminiscent of some type of

low-dimensional localized spin system. Below 13 K, the value of χ increases again, probably owing to a paramagnetic impurity. Assuming that the paramagnetic impurity obeys Curie's law, the amount of paramagnetic impurity was estimated as 0.76%. The magnetic data were analyzed by the Bonner−Fisher model (Eq. 2),[13] which describes an antiferromagnetic uniform chain with S = 1/2 spins, and by a modified model incorporating interchain interactions (Eq. 3):[14]

$$\chi_{BF} = f \frac{0.25 + 0.14995X + 0.30049X^2}{1 + 1.9862X + 0.68854X^2 + 6.0626X^3} \quad (2)$$

$$\chi = f \frac{\chi_{BF}}{1 - \frac{2zJ'\chi_{BF}}{N_A g^2 \mu_B^2}} \quad (3)$$

where $X = |J|/k_BT$, J' is the interchain interaction term, and z is the number of nearest neighbors. The best-fit parameters are $|J|/k_B$ = 70.5 K and f = 0.742 by Eq. 2 (Fig. S7) and $|J|/k_B$ = 67.1 K, zJ'/k_B = −61.1 K, and f = 0.799 by Eq. 3 (Fig. 5), where the value of g was fixed as 2 during the fitting process. Eq. 3 implies that both intrachain and interchain magnetic interactions (J and J') are antiferromagnetic.

Normal-mode analysis and vibrational spectroscopy

At the B3LYP/Aug-cc-pVTZ(-PP) level of theory, a full geometry optimization and normal-mode analysis for neutral EDO-TTF-I^0 and monocationic EDO-TTF-I$^{\bullet+}$ were conducted, and the calculated C=C stretching modes (ν_6, ν_7, and ν_8 modes) are illustrated in Fig. 6. In EDO-TTF-I^0, the ν_6 mode is considered to be the C=C stretching of a 1,3-dithiole ring with an ethylenedioxy group, while the ν_7 and ν_8 modes are the out-of-phase and in-phase C=C stretching of a 1,3-dithiole ring and bridge, respectively. According to Fig. 6, the manner of mode mixing slightly changes upon one-electron oxidation, and the C=C stretching modes of the 1,3-dithiole rings with and without the ethylenedioxy group are mixed in the ν_6 mode. Moreover, the frequency shifts upon oxidation are not the same among the ν_6, ν_7, and ν_8

modes. However, the outstanding frequency shifts upon oxidation can be utilized to estimate the molecular charge as well as the other molecular conductors.[15]

The infrared and Raman spectra of EDO-TTF-I along with the theoretical spectra are shown in Fig. S8. The present theoretical calculation reproduces the observed spectra well when a frequency scaling factor of 0.969 is applied. The assignments of the experimentally observed bands are summarized in Table S2. In both the infrared and Raman spectra of EDO-TTF-I, the CH_2 scissoring and wagging modes are observed in addition to the C=C stretching modes of ν_6, ν_7, and ν_8 in the spectral region. However, these modes are observed at much weaker intensities than the C=C stretching modes. Therefore, we can confidently distinguish the C=C stretching modes from the other modes.

The temperature-variable Raman spectra of $(EDO\text{-}TTF\text{-}I)_2PF_6$ are shown in Fig. 7. Three intense bands are observed at 1587, 1507, and 1465 cm^{-1} at 300 K. Compared with the theoretical spectra of $EDO\text{-}TTF\text{-}I^0$ and $EDO\text{-}TTF\text{-}I^{\bullet+}$, these bands are assignable to the ν_6, ν_7, and ν_8 modes, respectively. No spectral splitting of the ν_6, ν_7, and ν_8 modes indicates that all EDO-TTF-I molecules have a homogeneous charge of +0.5 based on the chemical composition, or the molecular charge difference is so small that Raman spectroscopy cannot detect it. Therefore, we rule out charge disproportionation in $(EDO\text{-}TTF\text{-}I)_2PF_6$. This is also consistent with the result that one EDO-TTF-I molecule is crystallographically unique. As the temperature decreases, the ν_6, ν_7, and ν_8 modes exhibit slight shifts that are less than 5 cm^{-1} to 1589, 1512, and 1470 cm^{-1}, respectively, at 5 K, accompanied by spectral narrowing. These results suggest that the molecular charge remains unchanged down to 5 K without charge disproportionation. The strong molecular dimerization is regarded to be the origin of the suppression of charge disproportionation by analogy with the abovementioned results for $(TMTTF)_2PF_6$ and $(TMTTF)_2AsF_6$.[12] Taking into account the results of the calculated band structure, electrical conductivity, magnetic properties, and Raman spectroscopy, $(EDO\text{-}TTF\text{-}I)_2PF_6$ is considered to be a dimerized Mott insulator.

Conclusions

An X-ray structural analysis and tight-binding band calculations revealed a strongly dimerized columnar structure with a β'-type molecular arrangement in (EDO-TTF-I)$_2$PF$_6$, where the iodine atom showed effective short I···F and I···S contacts between an EDO-TTF-I molecule and a PF$_6$ anion and between EDO-TTF-I molecules. The band consisting of the HOMOs split into two bands owing to this strong molecular dimerization, and the upper band is effectively half-filled. The salt showed semiconducting behavior and magnetic properties characteristic of a low-dimensional localized spin system, which was analyzed by the modified Bonner−Fisher model with interchain interaction. Along with the results obtained by temperature-variable Raman spectroscopy, (EDO-TTF-I)$_2$PF$_6$ is considered to be a dimerized Mott insulator in the range of 5−300 K.

Experimental and computational

General

Dry THF was obtained from Kanto Chemical. Perfluorohexyl iodide and 2.0-M LDA in THF/heptane/ethylbenzene were purchased from Aldrich. EDO-TTF was prepared according to the literature.[8] For electrocrystallization, ethanol was distilled from Mg/I$_2$ in an argon atmosphere, and (TBA)PF$_6$ was purified by recrystallization from ethanol. ^{1}H and ^{13}C NMR spectra were measured using a JEOL JNM-ECA600 spectrometer. The chemical shift was recorded relative to an internal TMS standard. X-ray diffraction images were acquired by the use of a Bruker SMART ApexII CCD diffractometer with graphite monochromated Mo Kα radiation at 300 and 100 K. Data reduction was performed by the Bruker SAINT program, and the multiscan absorption correlation was applied. The space group was determined by the Xprep program. The structural solution was obtained utilizing the Yadokari-XG interface.[16] The structures were solved by SIR-2014[17] and refined by SHELXL-2014.[18] Hydrogen atoms were introduced at the calculated positions (riding model). The electrical resistivities of (EDO-TTF-I)$_2$PF$_6$ single crystals were measured by the four-probe method. The gold wires were bonded to the sample surface by using carbon paste (DOTITE XC-12). The magnetic susceptibilities of the polycrystalline samples were measured in a 5000-Oe field by a Quantum Design MPMS-XL system.

The raw data were corrected for both the magnetization of the sample holder alone and the diamagnetic contribution of sample itself. The diamagnetic contribution was estimated by using Pascal's constants: $\chi_{dia} = -378.74\times10^{-6}$ emu mol^{-1}. Infrared spectra of KBr pellets were acquired with a Perkin-Elmer Spectrum 400 spectrophotometer. Raman spectra were measured using a Renishaw Raman microscope system in the 180° backreflecting geometry. The sample was irradiated by a 633-nm laser. The intensity of the excitation light was reduced below 100 μW to avoid sample heating and radiation damage.

Synthesis of 4,5-ethylenedioxy-4'-iodotetrathiafulvalene (EDO-TTF-I)

To a solution of EDO-TTF (1.00 g, 3.81 mmol) in dry THF (100 mL), 2.0-M LDA in THF/heptane/ethylbenzene (2 mL, 4.0 mmol) was added for 4 min in an argon atmosphere at −78 °C. After stirring at −78 °C for 1 h, perfluorohexyl iodide (3.0 mL, 13 mmol) was added for 17 min. The resulting mixture was stirred at −78 °C for 1.5 h and then allowed to room temperature. Saturated NH_4Cl_{aq} (150 mL) was added to the resulting mixture, which was extracted with CS_2 and washed with saturated $NaCl_{aq}$. The organic layer was dried over $MgSO_4$, and the solvent was evaporated. The residue was chromatographed on silica gel with CS_2 as eluent, where purification by chromatography was performed twice, to afford a brown oil. Acetonitrile was added to the oil and cooled. A black powdery solid was removed by filtration, and the filtrate was evaporated to afford EDO-TTF-I as a red solid (1.07 g, 72%). EDO-TTF-I was further purified by recrystallization from acetonitrile and used for the following experiments. mp 81−82 °C (decomp.) (lit.,[8] 78−79 °C (decomp.)); ^{1}H NMR (600 MHz, $CDCl_3$) δ 4.37 (4H, s), 6.46 (1H, s); ^{13}C NMR (150 MHz, $CDCl_3$) δ 63.7, 66.2, 100.7, 116.8, 123.1, 123.2, 124.0 (Only seven signals were observed, probably owing to the overlap of two signals assigned to *C*−I and *C*H_2 at 66.2 ppm. This is supported by the fact that the signal at 66.2 ppm is stronger than that at 63.7 ppm and by the literature,[8] which indicates that diiodonated EDO-TTF-I_2 shows two signals assigned to *C*H_2 and *C*−I at 66.1 and 77.2 ppm.); Calc. for $C_8H_5IO_2S_4$: C, 24.75; H, 1.30; I, 32.68; O, 8.24; S, 33.03. Found: C, 24.81; H, 1.29; I, 32.49; O, 8.28; S, 33.15%.

Electrocrystallization of (EDO-TTF-I)$_2$PF$_6$

(EDO-TTF-I)$_2$PF$_6$ was prepared by the electrocrystallization of EDO-TTF-I in an H-shaped electrochemical cell with a glass frit separating the anode and cathode arms. Typically, EDO-TTF-I (*ca*. 16 mg) was placed in the anode arm of the cell and (TBA)PF$_6$ (*ca*. 32 mg) in each arm, which was then filled with absolute ethanol (18 mL). The mixture was stirred to give a homogeneous solution. Using Pt electrodes (2 and 1 mm in diameter for the anode and cathode, respectively), galvanostatic electrolysis (0.5 μA) for less than two weeks at room temperature afforded black platelets on the anode electrode. The most developed crystal face was the (001) surface elongated along the *b* axis.

Computational

The HOMO of the EDO-TTF-I molecule and the intermolecular overlap integrals between HOMOs were estimated on the basis of the extended Hückel method. The transfer integral (t) was assumed to be proportional to the overlap integral (s) between HOMOs and estimated as $t = Es$ ($E = -10$ eV). Using these transfer integrals, the band structure was calculated within the tight-binding approximation. The parameters of the atomic orbitals were taken from the literature.[19,20] The calculations were carried out without and with the sulfur 3d orbitals in order to investigate the parameter dependence. The program developed by Mori *et al*.[19] was used.

Density functional theory calculations based on the B3LYP functional[21] were performed using the Aug-cc-pVTZ (C, H, O, and S atoms)[22] and Aug-cc-pVTZ-PP (I atom)[23] basis sets. For the full geometry optimizations and frequency calculations for EDO-TTF-I^0 and EDO-TTF-I$^{\bullet+}$, both “Opt = Tight” and “Int = UltraFine” were specified. All density functional theory calculations were performed using the Gaussian 09 program package.[24]

Conflicts of interest

There are no conflicts to declare.

Acknowledgments

This work was partly supported by a Grant-in-Aid for Scientific Research on Innovative Areas, "π-System Figuration: Control of Electron and Structural Dynamism for Innovative Functions," from the Japan Society for the Promotion of Science (JSPS) JP17H05153 and by JSPS KAKENHI, grant numbers JP15K17901 and JP26288035. Elemental analyses were performed at the Organic Elemental Microanalysis Laboratory, Kyoto University. Raman spectroscopy was conducted at the Institute for Molecular Science, supported by the Nanotechnology Platform Program (Molecule and Material Synthesis) of the Ministry of Education, Culture, Sports, Science and Technology (MEXT), Japan. The computations were performed using the Research Center for Computational Science, Okazaki, Japan.

Notes and references

1 M. Fourmigué and P. Batail, *Chem. Rev.*, 2004, **104**, 5379.

2 A. Mukherjee, S. Tothadi and G. R. Desiraju, *Acc. Chem. Res.*, 2014, **47**, 2514; G. Cavallo, P. Metrangolo, T. Pilati, G. Resnati and G. Terraneo, *Cryst. Growth Des.*, 2014, **14**, 2697; P. Politzer, J. S. Murray, G. V. Janjić and S. D. Zarić, *Crystals*, 2014, **4**, 12.

3 A. L. Allred and E. G. Rochow, *J. Inorg. Nucl. Chem.*, 1958, **5**, 264.

4 K. S. Shin, O. Jeannin, M. Brezgunova, S. Dahaoui, E. Aubert, E. Espinosa, P. Auban-Senzier, R. Świetlik, A. Frąckowiakd and M. Fourmigué, *Dalton Trans.*, 2014, **43**, 5280; J. Lieffrig, R. Le Pennec, O. Jeannin, P. Auban-Senzier and M. Fourmigué, *CrystEngComm*, 2013, **15**, 4408; M. Brezgunova, K. S. Shin, P. Auban-Senzier, O. Jeannin and M. Fourmigué, *Chem. Commun.*, 2010, **46**, 3926; J Lieffrig, O. Jeannin, A. Frąckowiak, I. Olejniczak, R. Świetlik, S. Dahaoui, E. Aubert, E. Espinosa, P. Auban-Senzier and M. Fourmigué, *Chem. Eur. J.*, 2013, **19**, 14804; K. S. Shin, M. Brezgunova, O. Jeannin, T. Roisnel, F. Camerel, P. Auban-Senzier and Marc Fourmigué, *Cryst. Growth Des.*, 2011, **11**, 5337; T. Devic, B. Domercq, P. Auban-Senzier, P. Molinié and M. Fourmigué, *Eur. J. Inorg. Chem.*, 2002, 2844; M. Fourmigué and P. Auban-Senzier, *Inorg. Chem.*, 2008, **47**, 9979; B. Domercq, T. Devic, M. Fourmigué, P. Auban-Senzier and E. Canadell, *J. Mater.*

Chem., 2001, **11**, 1570; A. Alberola, M. Fourmigué, C. J. Gómez-García, R. Llusar and S. Triguero, *New J. Chem.*, 2008, **32**, 1103.

5 a) A. Łapiński, R. Świetlik, M. Polomska, L. Ouahab and T. Imakubo, *J. Low Temp. Phys.*, 2006, **142**, 597; b) L. Ouahab, F. Setifi, S. Golhen, T. Imakubo, R. Lescouëzec, F. Lloret, M. Julve and R. Świetlik, *C. R. Chimie*, 2005, **8**, 1286; c) M. Tamura, K. Yamanaka, Y. Mori, Y. Nishio, K. Kajita, H. Mori, S. Tanaka, J. -I. Yamaura, T. Imakubo, R. Kato, Y. Misaki and K. Tanaka, *Synth. Met.*, 2001, **120**, 1041; d) T. Imakubo, T. Shirahata, K. Hervé and L. Ouahab, *J. Mater. Chem.*, 2006, **16**, 162; e) T. Imakubo, N. Tajima, M. Tamura, R. Kato, Y. Nishio and K. Kajita, *J. Mater. Chem.*, 2002, **12**, 159; f) T. Imakubo, T. Shirahata, M. Kibune and H. Yoshino, *Eur. J. Inorg. Chem.*, 2007, 4727; g) T. Imakubo and M. Kobayashi, *Eur. J. Inorg. Chem.*, 2014, 3973; h) T. Shirahata, M. Kibune, M. Maesato, T. Kawashima, G. Saito and T. Imakubo, *J. Mater. Chem.*, 2006, **16**, 3381; i) T. Imakubo and R. Murayama, *CrystEngComm*, 2013, **15**, 3072; j) T. Imakubo, M. Kibune, H. Yoshino, T. Shirahata and K. Yoza, *J. Mater. Chem.*, 2006, **16**, 4110.

6 a) Y. Kuwatani, E. Ogura, H. Nishikawa, I. Ikemoto and M. Iyoda, *Chem. Lett.*, 1997, 817; b) J. Nishijo, E. Ogura, J. Yamaura, A. Miyazaki, T. Enoki, T. Takano, Y. Kuwatani and M. Iyoda, *Solid State Commun.*, 2000, **116**, 661; c) J. Nishijo, E. Ogura, J. Yamaura, A. Miyazaki, T. Enoki, T. Takano, Y. Kuwatani and M. Iyoda, *Synth. Met.*, 2003, **133-134**, 539; d) A. Miyazaki, K. Enomoto, K. Okabe, H. Yamazaki, J. Nishijo, T. Enoki, E. Ogura, K. Ugawa, Y. Kuwatani and M. Iyoda, *J. Solid State Chem.*, 2002, **168**, 547; e) U. Kux, H. Suzuki, S. Sasaki and M. Iyoda, *Chem. Lett.*, 1995, 183.

7 a) A. Ota, H. Yamochi and G. Saito, *J. Mater. Chem.*, 2002, **12**, 2600; b) M. Chollet, L. Guerin, N. Uchida, S. Fukaya, H. Shimoda, T. Ishikawa, K. Matsuda, T. Hasegawa, A. Ota, H. Yamochi, G. Saito, R. Tazaki, S. Adachi and S. Koshihara, *Science*, 2005, **307**, 86; c) K. Onda, S. Ogihara, K. Yonemitsu, N. Maeshima, T. Ishikawa, Y. Okimoto, X. F. Shao, Y. Nakano, H. Yamochi, G. Saito and S. Koshihara, *Phys. Rev. Lett.*, 2008, **101**, 067403; d) Y. Nakano, H. Yamochi, G. Saito, M. Uruichi and K. Yakushi, *J. Phys.: Conf. Ser.*, 2009, **148**, 012007; e) N. Fukazawa, M. Shimizu, T.

Ishikawa, Y. Okimoto, S. Koshihara, T. Hiramatsu, Y. Nakano, H. Yamochi, G. Saito and K. Onda, *J. Phys. Chem. C*, 2012, **116**, 5892; f) M. Gao, C. Lu, H. Jean-Ruel, L. C. Liu, A. Marx, K. Onda, S. Koshihara, Y. Nakano, X. F. Shao, T. Hiramatsu, G. Saito, H. Yamochi, R. R. Cooney, G. Moriena, G. Sciaini and R. J. D. Miller, *Nature*, 2013, **496**, 343; g) Y. Matsubara, S. Ogihara, J. Itatani, N. Maeshima, K. Yonemitsu, T. Ishikawa, Y. Okimoto, S. Koshihara, T. Hiramatsu, Y. Nakano, H. Yamochi, G. Saito and K. Onda, *Phys. Rev. B*, 2014, **89**, 161102(R); h) M. Servol, N. Moisan, E. Collet, H. Cailleau, W. Kaszub, L. Toupet, D. Boschetto, T. Ishikawa, A. Moréac, S. Koshihara, M. Maesato, M. Uruichi, X. F. Shao, Y. Nakano, H. Yamochi, G. Saito and M. Lorenc, *Phys. Rev. B*, 2015, **92**, 024304; i) L. Chung Liu, Y. Jiang, H. M. Mueller-Werkmeister, C. Lu, G. Moriena, M. Ishikawa, Y. Nakano, H. Yamochi and R. J. D. Miller, *Chem. Phys. Lett.*, 2017, **683**, 160; j) K. Onda, H. Yamochi and S. Koshihara, *Acc. Chem. Res.*, 2014, **47**, 3494.

8 M. Iyoda, Y. Kuwatani, E. Ogura, K. Hara, H. Suzuki, T. Takano, K. Takeda, J. Takano, K. Ugawa, M. Yoshida, H. Matsuyama, H. Nishikawa, I. Ikemoto, T. Kato, N. Yoneyama, J. Nishijo, A. Miyazaki and T. Enoki, *Heterocycles*, 2001, **54**, 833.

9 T. Mori, *Bull. Chem. Soc. Jpn.*, 1998, **71**, 2509.

10 T. Imakubo, H. Sawa and R. Kato, *Synth. Met.*, 1995, **73**, 117.

11 J. P. Pouget and S. Ravy, *J. Phys. I France*, 1996, **6**, 1501; Y. Nakano, T. Nishi, M. Uruichi, K. Yakushi and H. Yamochi, *Physica B*, 2010, **405**, S49.

12 Y. Nogami, T. Ito, K. Yamamoto, N. Irie, S. Horita, T. Kambe, N. Nagao, K. Oshima, N. Ikeda and T. Nakamura, *J. Phys. IV France*, 2005, **131**, 39.

13 J. C. Bonner and M. E. Fisher, *Phys. Rev. A*, 1964, **135**, 640; W. E. Hatfield, R. R. Weller and J. W. Hall, *Inorg. Chem.*, 1980, **19**, 3825.

14 W. E. Estes, D. P. Gavel, W. E. Hatfield and D. J. Hodgson, *Inorg. Chem.*, 1978, **17**, 1415.

15 S. Matsuzaki, R. Kuwata and K. Toyoda, *Solid State Commun.*, 1980, **33**, 403; S. Matsuzaki, T. Moriyama and K. Toyoda, *Solid State Commun.*, 1980, **34**, 857; S. Matsuzaki, T. Moriyama, M. Onomichi and K. Toyoda, *Bull. Chem. Soc. Jpn.*, 1983, **56**, 369; H. H. Wang, J. R. Ferraro, J. M.

Williams, U. Geiser and J. A. Schlueter, *J. Chem. Soc., Chem. Commun.*, 1994, 1893; O. Drozdova, H. Yamochi, K. Yakushi, M. Uruichi, S. Horiuchi and G. Saito, *J. Am. Chem. Soc.*, 2000, **122**, 4436; T. Yamamoto, M. Uruichi, K. Yamamoto, K. Yakushi, A. Kawamoto and H. Taniguchi, *J. Phys. Chem. B*, 2005, **109**, 15226; X. F. Shao, Y. Nakano, M. Sakata, H. Yamochi, Y. Yoshida, M. Maesato, M. Uruichi, K. Yakushi, T. Murata, A. Otsuka, G. Saito, S. Koshihara and K. Tanaka, *Chem. Mater.*, 2008, **20**, 7551; Y. Nakano, T. Nishi, M. Uruichi, K. Yakushi and H. Yamochi, *Physica B*, 2010, **405**, S49.

16 K. Wakita (2001). Yadokari-XG. Software for Crystal Structure Analyses. Release of Software (Yadokari-XG 2009) for Crystal Structure Analyses, C. Kabuto, S. Akine, T. Nemoto and E. Kwon, *J. Cryst. Soc. Jpn.*, 2009, **51**, 218.

17 M. C. Burla, R. Caliandro, B. Carrozzini, G. L. Cascarano, C. Cuocci, C. Giacovazzo, M. Mallamo, A. Mazzone and G. Polidori, *J. Appl. Cryst.*, 2015, **48**, 306.

18 G. M. Sheldrick, *Acra Cryst.*, 2008, **A64**, 112.

19 T. Mori, A. Kobayashi, Y. Sasaki, H. Kobayashi, G. Saito and H. Inokuchi, *Bull. Chem. Soc. Jpn.*, 1984, **57**, 627.

20 R. S. Summervile and R. Hoffmann, *J. Am. Chem. Soc.*, 1976, **98**, 7240.

21 A. D. Becke, *J. Chem. Phys.*, 1993, **98**, 5648.

22 T. H. Dunning, Jr., *J. Chem. Phys.*, 1989, **90**, 1007; D. E. Woon and T. H. Dunning, Jr., *J. Chem. Phys.*, 1993, **98**, 1358.

23 K. A. Peterson, B. C. Shepler, D. Figgen and H. Stoll, *J. Phys. Chem. A*, 2006, **110**, 13877; D. Feller, *J. Comp. Chem.*, 1996, **17**, 1571; K. L. Schuchardt, B. T. Didier, T. Elsethagen, L. Sun, V. Gurumoorthi, J. Chase, J. Li and T. L. Windus, *J. Chem. Inf. Model.*, 2007, **47**, 1045.

24 Gaussian 09, Revision D.01, M. J. Frisch, G. W. Trucks, H. B. Schlegel, G. E. Scuseria, M. A. Robb, J. R. Cheeseman, G. Scalmani, V. Barone, B. Mennucci, G. A. Petersson, H. Nakatsuji, M. Caricato, X. Li, H. P. Hratchian, A. F. Izmaylov, J. Bloino, G. Zheng, J. L. Sonnenberg, M. Hada, M. Ehara, K. Toyota, R. Fukuda, J. Hasegawa, M. Ishida, T. Nakajima, Y. Honda, O. Kitao, H. Nakai, T.

Vreven, J. A. Montgomery, Jr., J. E. Peralta, F. Ogliaro, M. Bearpark, J. J. Heyd, E. Brothers, K. N. Kudin, V. N. Staroverov, T. Keith, R. Kobayashi, J. Normand, K. Raghavachari, A. Rendell, J. C. Burant, S. S. Iyengar, J. Tomasi, M. Cossi, N. Rega, J. M. Millam, M. Klene, J. E. Knox, J. B. Cross, V. Bakken, C. Adamo, J. Jaramillo, R. Gomperts, R. E. Stratmann, O. Yazyev, A. J. Austin, R. Cammi, C. Pomelli, J. W. Ochterski, R. L. Martin, K. Morokuma, V. G. Zakrzewski, G. A. Voth, P. Salvador, J. J. Dannenberg, S. Dapprich, A. D. Daniels, O. Farkas, J. B. Foresman, J. V. Ortiz, J. Cioslowski and D. J. Fox, Gaussian, Inc., Wallingford CT, 2013.

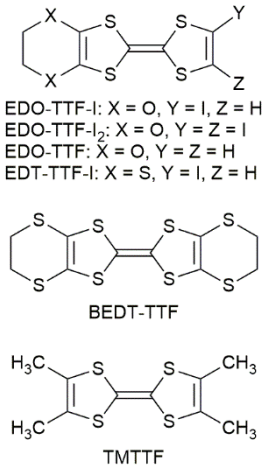

Chart 1 Molecular structures.

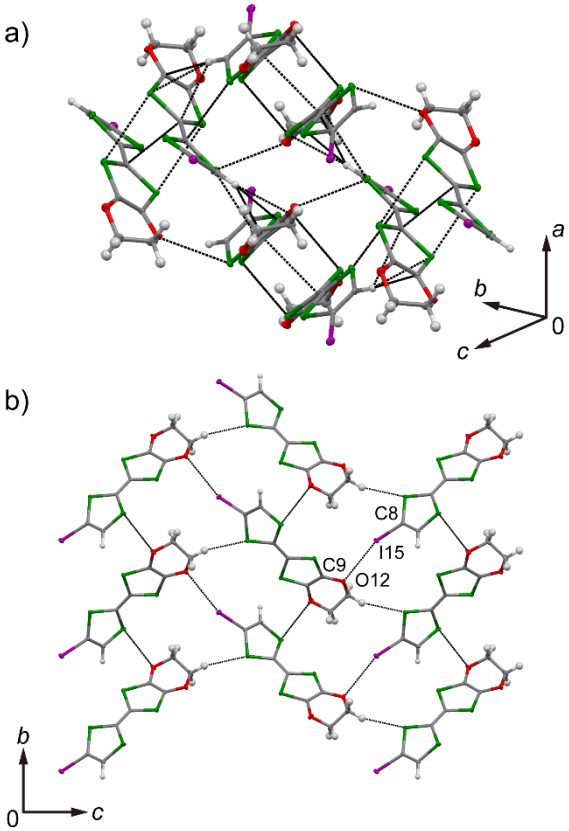

Fig. 1 Short atomic contacts at (a) z = 0.5 and (b) x = 0 in EDO-TTF-I at 100 K.

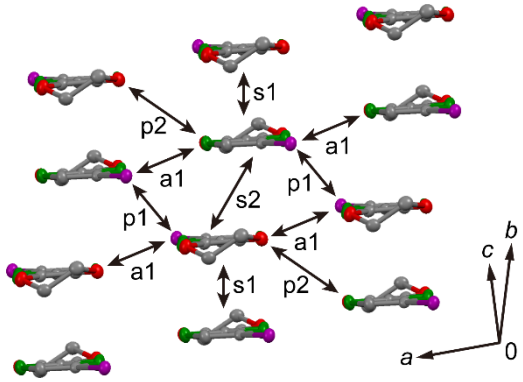

Fig. 2 Molecular arrangement in (EDO-TTF-I)$_2$PF$_6$ at 300 K and the notation for the intermolecular overlap integrals between HOMOs.

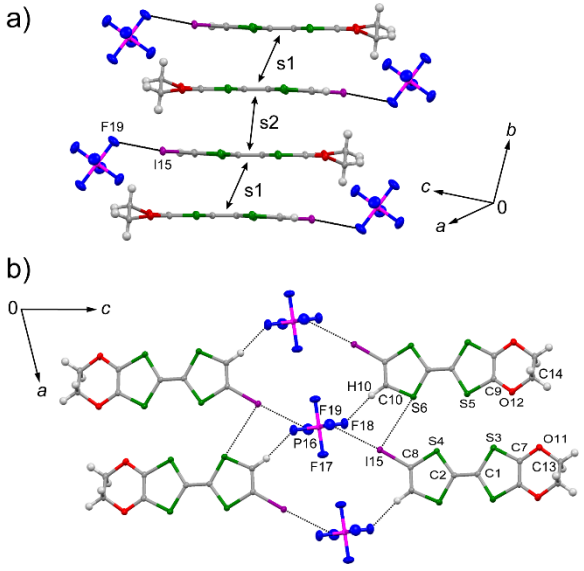

Fig. 3 (a) Dimerized stacking column in a head-to-tail manner and (b) short atomic contacts in (EDO-TTF-I)$_2$PF$_6$ at 300 K along with the atomic numbering. The ring-over-bond and ring-over-atom overlapping modes correspond to the *s*1 and *s*2 interactions, respectively (*s*1 > *s*2).

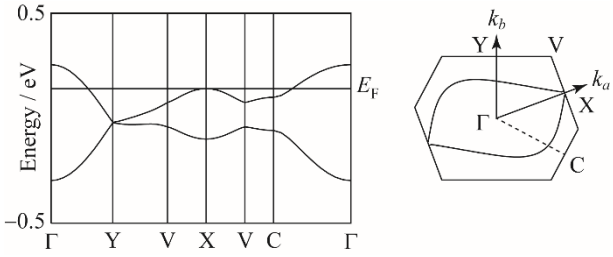

Fig. 4 Energy band structure and Fermi surface at 300 K. The contribution of the sulfur 3d orbitals is not included in the calculation.

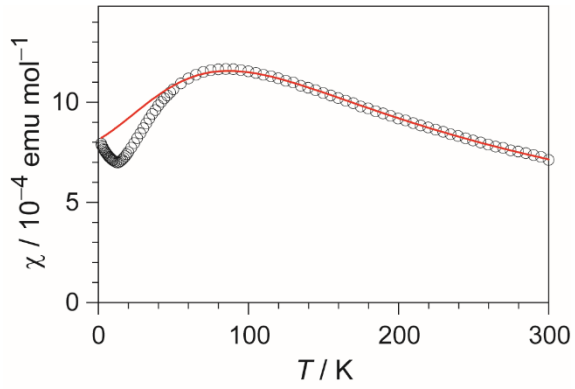

Fig. 5 Temperature dependence of the magnetic susceptibility (χ) of $(EDO\text{-}TTF\text{-}I)_2PF_6$. The solid curve represents the best fit to the Bonner−Fisher model with interchain magnetic interactions (see text).

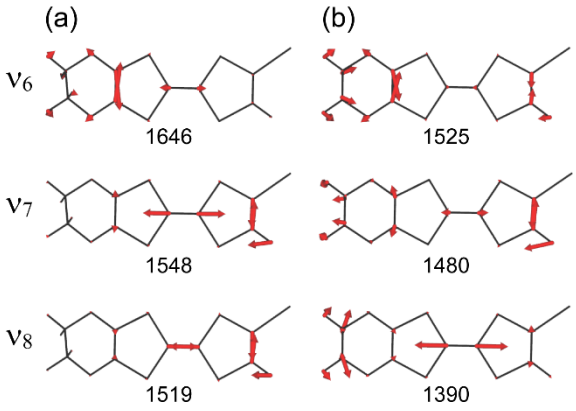

Fig. 6 C=C stretching modes of (a) EDO-TTF-I^0 and (b) EDO-TTF-$I^{\bullet+}$ at the B3LYP/Aug-cc-pVTZ(-PP) level of theory. The calculated frequencies (cm^{-1}) are shown below the corresponding vibrational modes, where the scaling factor is 0.969.

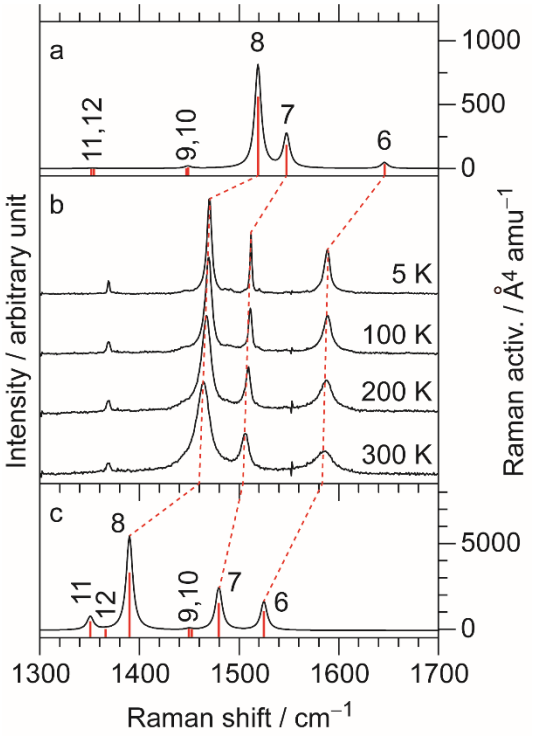

Fig. 7 Temperature dependence of the Raman spectra in $(EDO\text{-}TTF\text{-}I)_2PF_6$: calculated Raman spectra for (a) EDO-TTF-I^0 and (c) EDO-TTF-$I^{\bullet+}$ at the B3LYP/aug-ccpVTZ(-PP) level of theory. The numbers correspond to *j* for the ν_j mode, and the frequency scaling factor is 0.969.

Table 1 Crystallographic data of EDO-TTF-I and $(EDO\text{-}TTF\text{-}I)_2PF_6$.

	EDO-TTF-I		$(EDO\text{-}TTF\text{-}I)_2PF_6$	
Empirical formula	$C_8H_5IO_2S_4$		$C_{16}H_{10}F_6I_2O_4PS_8$	
Formula weight	388.26		921.49	
Crystal color	deep orange		black	
Crystal dimensions	0.24×0.20×0.04		0.12×0.11×0.03	
Temperature (K)	100	300	100	300
Crystal system	Orthorhombic	Orthorhombic	Triclinic	Triclinic
Space group	*Pbca* (#61)	*Pbca* (#61)	$P\bar{1}$ (#2)	$P\bar{1}$ (#2)
Lattice parameter				
a (Å)	8.1944(5)	8.3903(6)	6.4961(6)	6.5423(9)
b (Å)	14.4974(8)	14.7805(11)	7.4115(7)	7.5209(11)
c (Å)	19.7587(11)	19.6241(15)	14.3958(13)	14.593(2)
α (°)	90	90	92.1840(10)	91.270(2)
β (°)	90	90	76.2630(10)	76.695(2)
γ (°)	90	90	110.4120(10)	110.167(2)
V (Å^3)	2347.3(2)	2433.6(3)	630.24(10)	654.65(16)
Z value	8	8	1	1
D_{calc} (g cm^{-3})	2.197	2.119	2.428	2.337
F_{000}	1488	1488	441	441
μ(Mo Kα) (mm^{-1})	3.414	3.293	3.293	3.170
Radiation (Å)	0.71073	0.71073	0.71073	0.71073
$2\theta_{max}$ (°)	58.706	58.468	58.22	54.04
No. independent reflections	13608	14141	2999	3116
No. reflections observed	3036	3161	3925	4072
No. parameters	127	136	169	169
R_{int}	0.0344	0.0496	0.0131	0.0161
R^a ($I > 2.0\sigma$)	0.0246	0.0419	0.0239	0.0341
Rw^b (all data)	0.0542	0.1043	0.0570	0.0724
Goodness-of-fit indicator, S^c	1.038	0.991	1.019	1.014
Max. shift/error in final cycle	0.000	0.000	0.000	0.000
Max. and min. peaks in final diff. map (e Å^{-3})	0.83, −0.68	1.10, −0.71	1.02, −0.48	0.70, −0.54
CCDC	1590291	1590292	1590293	1590294

[a] $R = \sum||F_o| - |F_c||/\sum|F_o|$. [b] $Rw = [\sum w(|F_o| - |F_c|)^2/\sum w|F_o|^2]^{1/2}$. [c] $S = [\sum w(|F_o| - |F_c|)^2/(N_o - N_p)]^{1/2}$, N_o: number of reflections observed, N_p: number of parameters.

Electronic Supplementary Information

Crystal structure and physical properties of radical cation salt based on 4,5-ethylenedioxy-4'-iodotetrathiafulvalene (EDO-TTF-I) with iodine bonding ability

Yoshiaki Nakano,*[ab] Yusuke Takahashi,[a] Kohdai Ishida,[a] Manabu Ishikawa,[b]

Hideki Yamochi[ab] and Mikio Uruichi[c]

[a.] Department of Chemistry, Graduate School of Science, Kyoto University, Kitashirakawa Oiwake-cho, Sakyo-ku, Kyoto 606-8502, Japan.

[b.] Research Center for Low Temperature and Materials Sciences, Kyoto University, Yoshida Honmachi, Sakyo-ku, Kyoto 606-8501, Japan.

[c.] Institute for Molecular Science, Myodaiji, Okazaki, Aichi 444-8585, Japan.

E-mail: nakano.yoshiaki.5x@kyoto-u.ac.jp (Y. Nakano).

(a)

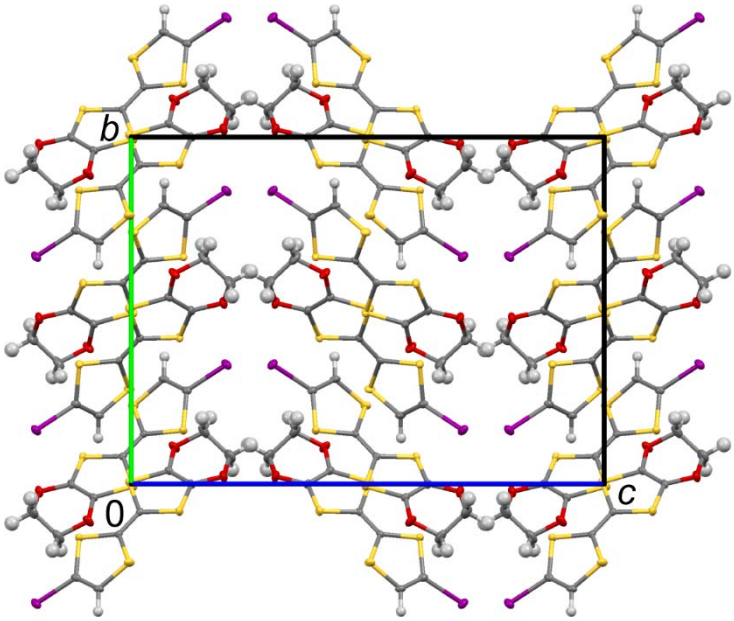

(b)

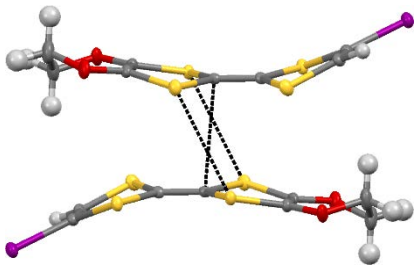

Fig. S1 (a) Crystal and (b) dimer structures of EDO-TTF-I at 100 K.

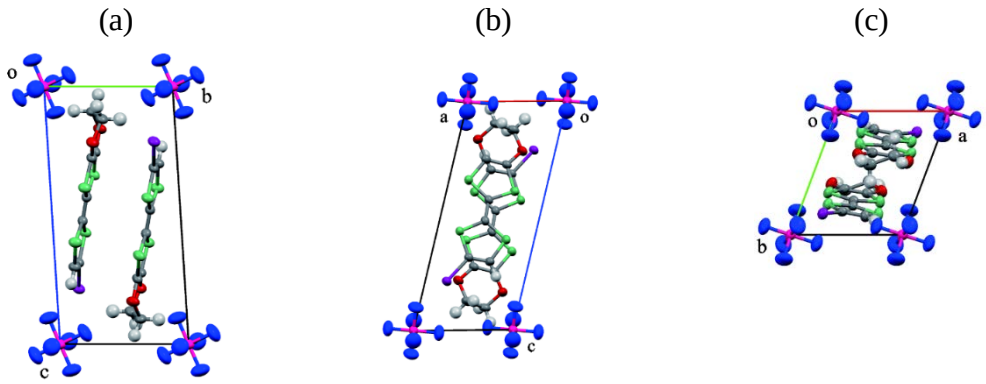

Fig. S2 Crystal structures viewed along (a) *a*, (b) *b*, and (c) *c* axes of $(EDO\text{-}TTF\text{-}I)_2PF_6$ at 300 K.

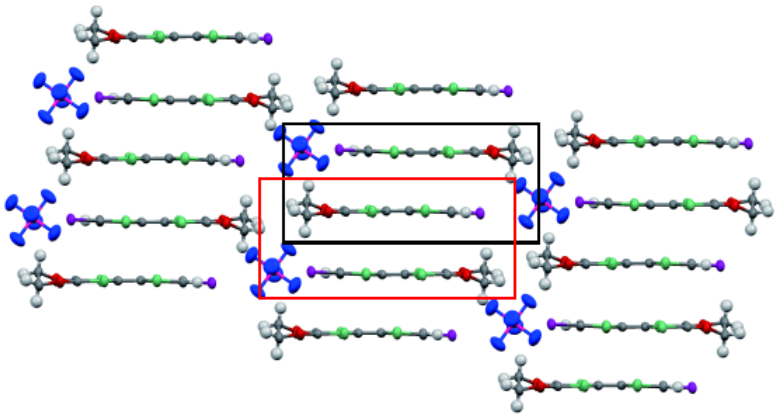

Fig. S3 Molecular packing viewed along molecular short axis in $(EDI\text{-}TTF\text{-}I)_2PF_6$ at 300 K. The boxes in black and red indicate the ring-over-bond and ring-over-atom stacking manners, respectively.

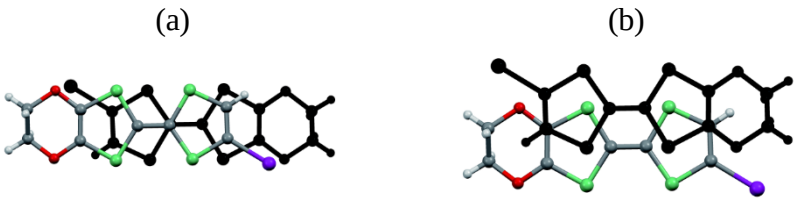

Fig. S4 Stacking manners viewed along stacking axis in $(EDI\text{-}TTF\text{-}I)_2PF_6$ at 300 K. (a) Ring-over-bond and (b) ring-over-atom manners.

Table S1 Overlap integrals (10^{-3}) calculated without and with sulfur 3d orbitals, degree of molecular dimerization ($\Delta s/\langle s\rangle$) and energy gaps between upper and lower bands

	Without sulfur 3d orbitals		With sulfur 3d orbitals	
	300 K	100 K	300 K	100 K
$s1$	11.9	13.2	22.9	25.8
$s2$	7.9	7.5	7.6	6.0
$a1$	1.0	1.4	4.0	5.2
$p1$	5.8	6.9	14.1	15.7
$p2$	2.0	2.1	6.9	7.4
$\Delta s/\langle s\rangle$[a]	0.40	0.55	1.00	1.24
E_g / eV	0.002	0.019	0.013	–

[a] $\Delta s/\langle s\rangle = 2(s1 - s2)/(s1 + s2)$.

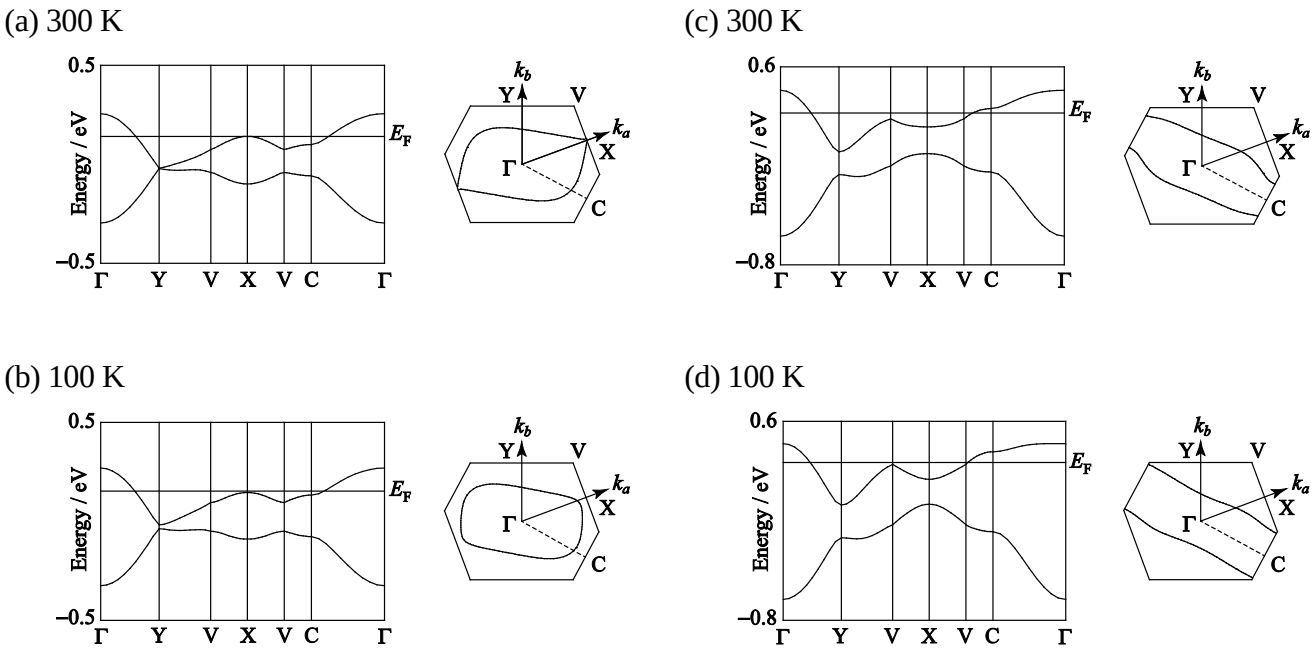

Fig. S5 Energy band structures and Fermi surfaces calculated (a, b) without and (c, d) with sulfur 3d orbitals.

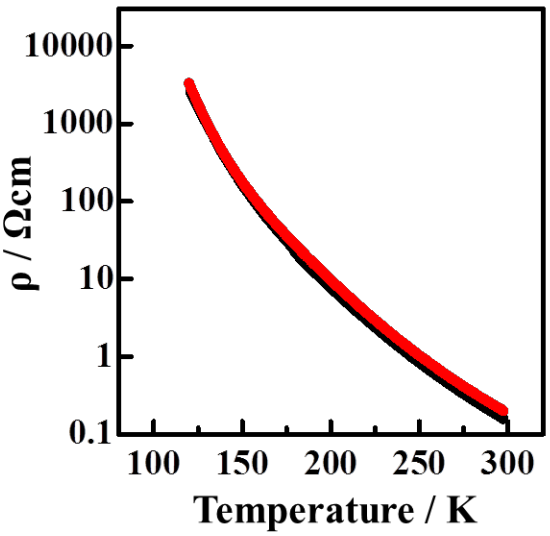

Fig. S6 Sample dependence on electrical resistivity measured along *b* axis in $(EDI\text{-}TTF\text{-}I)_2PF_6$. Two samples showed almost the same behavior.

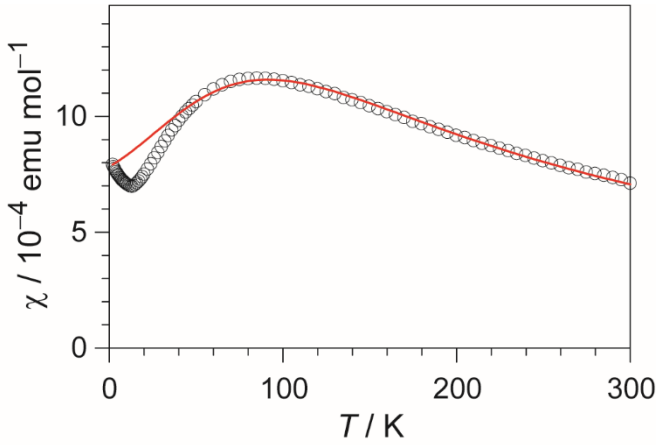

Fig. S7 Temperature dependence of the magnetic susceptibility (χ) of $(EDO\text{-}TTF\text{-}I)_2PF_6$. The solid curve represents the best fit to the Bonner−Fisher model.

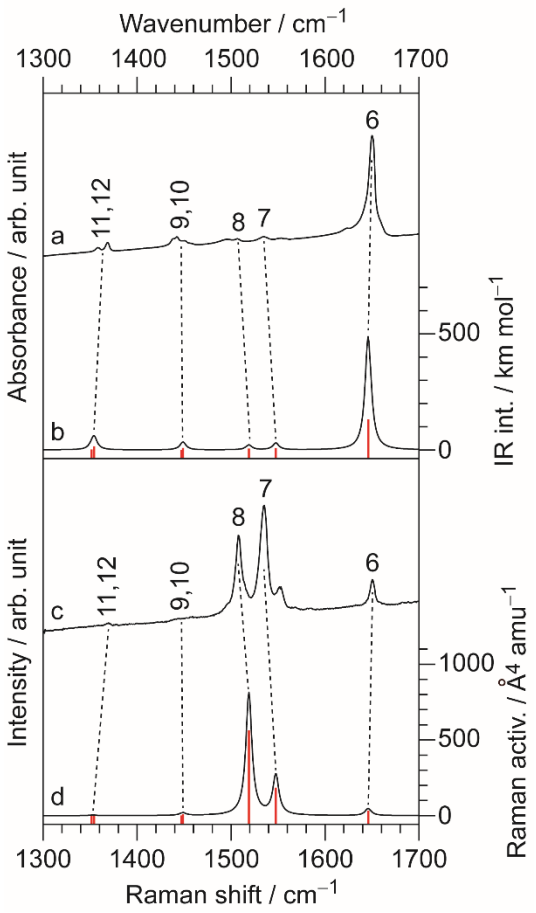

Fig. S8 (a) Observed infrared spectra of neutral EDO-TTF-I dispersed in KBr at room temperature. (c) Observed Raman spectra of neutral EDO-TTF-I excited by a 633-nm laser at 300 K. (b) Infrared spectra and (d) Raman spectra EDO-TTF-I^0 molecule calculated at the B3LYP/Aug-cc-pVTZ(-PP). The numbering *j* denotes the ν_j mode. The frequency scaling factor is 0.969.

Table S2 Observed and calculated frequencies (cm^{-1}) of EDO-TTF-I

v	Infrared	Raman	Calc.[a]	Assignment
6	1650	1650	1646	C=C stretching
7	1535	1535	1548	C=C stretching
8	1507	1508	1519	C=C stretching
9	1464	1463	1449	CH_2 scissoring
10	1451	1454	1447	CH_2 scissoring
	1443	1445		
11	1369	1369	1354	CH_2 wagging
12	1366	1365	1352	CH_2 wagging

[a] B3LYP/Aug-cc-pVTZ(-PP), frequency scaling factor = 0.969.